Detection and attribution of reference evapotranspiration change (1951–2020) in the Upper Yangtze River Basin of China

Manlin Wang, Yu Zhang, Yan Lu, Xulong Gong and Li Gao

ABSTRACT

Reference evapotranspiration (ET_0) indicates atmospheric evaporating capability over a hypothetical reference surface. ET_0 is an important hydrological and meteorological variable to reflect climate change. This is particularly true for the Upper Yangtze River Basin (UYRB), which is vulnerable and sensitive to changing environment. This study aims to provide a newer and longer description of ET_0 change and the causes at basin and subbasin scales in the UYRB. Based on the observed data from 1951 to 2020, ET_0 in the entire UYRB and subbasins is estimated using the Penman–Montieth method with local calibration. The spatial–temporal characteristics in ET_0 change are identified from time-series analysis. Our results show that ET_0 increases significantly by 3.3 mm/year in the entire UYRB. Stations with significant increases in annual ET_0 are concentrated in the central part of the UYRB, where the mean annual ET_0 is low. We further propose an improved method to assess the causes of ET_0 change. Our results suggest that the relative humidity decrease has the most dominant effect, causing 4.69 mm/year of ET_0 increase. Temperature increase tends to cause 1.26 mm/year of ET_0 increase. Sunshine duration decrease and wind speed decrease contribute to 1.96 and 0.48 mm/year of ET_0 decrease.

Key words | attribution analysis, climate change, reference evapotranspiration change, sensitivity analysis, the Upper Yangtze River Basin

Manlin Wang
Yan Lu
Xulong Gong
Li Gao
Geological Survey of Jiangsu Province,
Nanjing 210018,
China
and
Key Laboratory of Earth Fissures Geological Disaster,
Ministry of Natural Resources,
Nanjing, 210018,
China

Yu Zhang (corresponding author)
State Key Laboratory of Hydrology – Water Resources and Hydraulic Engineering,
Nanjing Hydraulic Research Institute,
Nanjing 210029,
China
E-mail: *zhangyu74@163.com*

HIGHLIGHTS

- ET_0 increases significantly in the UYRB.
- The significant increases of annual ET_0 gather in the central region of the UYRB.
- The relative humidity decrease has the most dominant effect on ET_0 increase in the UYRB.
- The ET_0 change and contributions of climatic variables vary in subbasins.

INTRODUCTION

Global climate change has occurred in recent decades (Sippel *et al.* 2020). Under climate change, regional hydrological cycles have changed in different degrees (Zhang *et al.* 2020). Evapotranspiration is a special hydro-climatic variable, which is a key process in the water cycle, as well as an important component of energy budget in the land–atmosphere interaction. It is the only term that links the water balance and energy balance (Xu *et al.* 2006). Therefore, the study of regional evapotranspiration change is helpful to understand the regional climate change and its impacts on the hydrological cycle (Song *et al.* 2018; Pour *et al.* 2020; Yaseen *et al.* 2020).

The terms commonly used to describe evapotranspiration include pan evaporation (E_{pan}), actual evapotranspiration

doi: 10.2166/wcc.2021.011

(ET_a), potential evapotranspiration (ET_p), and reference evapotranspiration (ET_0). E_{pan} is the evaporation from the free water surface of an evaporation pan, which is the most direct observation for evaporation. The pan evaporation method has been used extensively to estimate evaporation from lakes and reservoirs. ET_a reveals the actual amount of evapotranspiration, which is the most complicated component of the water cycle. It depends on climatic factors, vegetation, soil, and amount of available water and is hard to measure (Yaseen *et al.* 2020). ET_p was first introduced by Thornthwaite (1948) and formally defined by Penman (1956) gave as 'the amount of water transpired in a given time by a short green crop, completely shading the ground, of uniform height and with adequate water status in the soil profile'. However, there is not an exact description of land-surface condition in this definition of ET_p. To make it more standardized and clearer, ET_0 was further introduced, which is defined as 'the rate of evapotranspiration from a hypothetical reference crop with an assumed crop height of 0.12 m, a fixed surface resistance of 70 s m^{-1} and an albedo of 0.23, closely resembling the evapotranspiration from an extensive surface of green grass of uniform height, actively growing, well-watered, and completely shading the ground' (Wang *et al.* 2012). ET_0 was further studied by researchers and recommended by the Food and Agriculture Organization (FAO). ET_0 describes the evaporation capacity of the atmosphere at a specific location and time and is able to be calculated directly from meteorological data. Furthermore, there is a good consistency between E_{pan} and ET_p (Ghorbani *et al.* 2018; Nourani *et al.* 2019), and the ET_a is usually estimated based on ET_0 (Nagler *et al.* 2013; Guo *et al.* 2016; Akhavan *et al.* 2019). Therefore, ET_0 is an excellent indicator for studying the evapotranspiration change and its causes (Jing *et al.* 2019). Statistical analysis and Geographic Information System (GIS) spatial analysis methods are commonly used in existing studies on the detection of spatial and temporal variability of ET_0. The recovered stationary series method is employed to assess the contribution of climatic variables to ET_0 change, which is employed as follows: (1) the trend in a climatic variable was removed to obtain a stationary time series; (2) ET_0 was recalculated by using the detrended data series, while original data for other variables were retained in each time; (3) the ET_0 values from the detrended and original time series were compared, and the difference was considered as the contribution of that variable to ET_0. However, when there is an abrupt change point in one climatic variable series, this method may misestimate the changes in climatic variables, especially when the time series is long (Xu *et al.* 2006; Qasem *et al.* 2019; Malik *et al.* 2020).

The Yangtze River is the longest river in Asia and the third-longest in the world. Water resources and hydropower resources of the Yangtze River are the most abundant in China. The Upper Yangtze River Basin (UYRB) is the streamflow formation area and hydropower storage area, accounting for 45% of basin water resources and 90% of basin hydropower resources, which has an irreplaceable position and inestimable value in China's strategic reserve of resources (Zhang *et al.* 2020). Recently, measured precipitation and runoff in most regions of the UYRB have been reported changing obviously, which has great impacts on economic development, social stability, and ecological security (Zhang *et al.* 2018; Qi *et al.* 2019; Qin *et al.* 2020; Zhong *et al.* 2020). The sensitivity of hydrological projection to ET_0 depends on climatic stage. Hydrological projection is generally more sensitive to ET_0 under humid climate (Weiland *et al.* 2012; Dakhlaoui *et al.* 2020). Therefore, identifying ET_0 change and assessing the contribution of climatic variables helps to understand the climate change and its impact on the hydrological cycle in the UYRB. Some scholars have conducted studies on the ET_0 change in the Yangtze River Basin. Xu *et al.* (2006) employed the Penman–Monteith method to analyze the spatial distribution and temporal trend of ET_0 and E_{pan} in the Yangtze River Basin based on the data from 1950 to 2000. Gong *et al.* (2006) analyzed the sensitivity of ET_0 to key climatic variables in the Yangtze River Basin during 1960–2000. Wang *et al.* (2007) investigated the upper and mid-lower Yangtze River basin trends of E_{pan} and ET_0 from 1961 to 2000 using daily data of 115 stations. Most previous studies were carried out on ET_0 change before 2000 in the Yangtze River Basin. The pattern of change may have varied due to climate change, making it difficult for the previous studies to explain the recent changes in the UYRB.

Recognizing the above concerns, in this study, the ET_0 in the UYRB during 1951–2020 is estimated by using the Penman–Montieth (Song *et al.* 2018) method. Spatiotemporal changes in ET_0 are detected to describe the regional climate change and its impact on the hydrological cycle.

We aim to use the newest data to update the existing studies mentioned above, providing a newer description of ET_0 change. An attribution analysis method is proposed to quantify the impacts of changes in climatic variables on ET_0. The sensitivity analysis is conducted to help further explore the causes of ET_0 change. Considering the extent of the paper, other forcings than the studied ones in the paper are not considered. This paper presents the early results of our ongoing study on adaptive regulation for the water resources system under changing environment. The results of ET_0 change provide important inputs of hydrological modeling under climate change.

STUDY AREA AND DATA PROCESSING

The UYRB is located between 90–112°E and 23–35°N, as shown in Figure 1, with a drainage area around 10,000 km^2. The UYRB experiences two different typical landforms. The western part is located over the Qinghai–Tibet Plateau and Hengduan Mountains with elevations higher than 3,000 m, while the southeastern part is located in the valley with elevations under 500 m. The complex landforms gave birth to the upper reaches of the Yangtze River. Based on the major rivers and watersheds, the UYRB is divided into the Jinsha River Basin (JSRB), the Mintuo River Basin (MTRB), the Jialing River Basin (JLRB), the Wujiang River Basin (WJRB) and the mainstream region (MSB). The average annual runoff ranges from 297.5 to 642.1 mm. The average annual precipitation ranges from 723.4 to 1,133.9 mm. The average annual temperature ranges from 8.6 to 16.8 °C.

Meteorological data from 80 National Meteorological Observatory stations within the UYRB are collected from the National Meteorological Information Centre of China, including daily observations of precipitation (*P*, mm), air

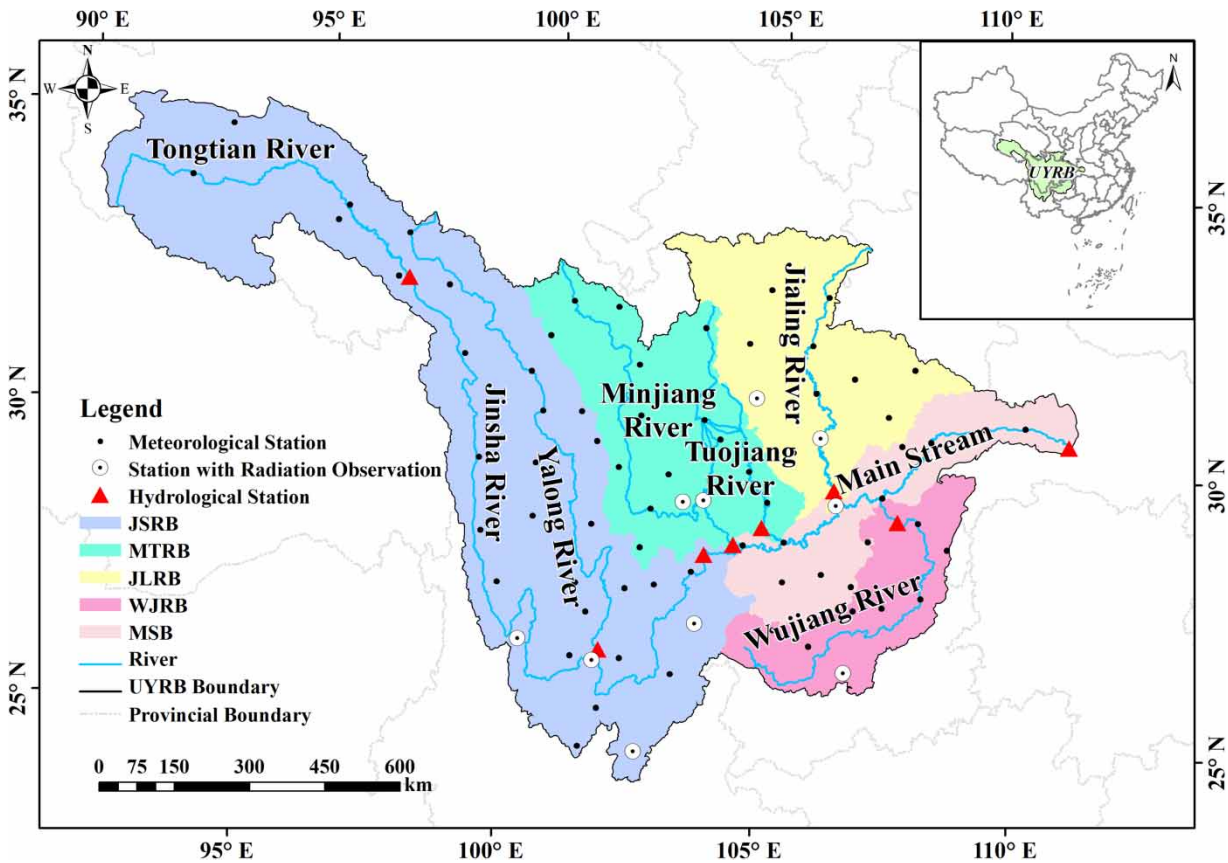

Figure 1 | Location of the UYRB and the meteorological stations.

temperature (T, °C), relative humidity (RH, %), wind speed (WS, m s^{-1}), and sunshine duration (SD, h) for the period from 1951 to 2020. The data have been subjected to strict quality control and inspection. Locations of the stations are shown in Figure 1. These stations are well distributed within the UYRB, which reflect the basin's climatic characteristics. Among these stations, 10 have well-recorded radiation observations and are used to calibrate the Angstrom coefficients for estimating the solar radiation in the Penman–Monteith method. More detailed information on these meteorological stations is listed in Table 1. The missing data (accounting for 0.6% of the total data) are interpolated by the average meteorological data from three neighboring stations.

METHODS

Penman–Montieth method

As mentioned in the 'Introduction' section, ET_0 is a theoretical climatic parameter, which reflects the evapotranspiration capacity of a basin under specific climatic conditions. Therefore, ET_0 change and the causes provide evidence of current climate change occurring and historic trends. There are a multitude of methods for the estimation of ET_0 (Xu & Singh 2002). Some of these methods are accurate and reliable; others provide only a rough approximation. Most of the methods were developed for use in specific studies and are most appropriate for use in climates similar to where they were developed (Xu *et al.* 2006). The Penman–Montieth method is considered to be the most reliable one among the ET_0 estimation methods, because it integrates both aerodynamic and physiological parameters (Xu *et al.* 2006). ET_0 is calculated by:

$$ET_0 = \frac{0.408\Delta(R_n - G) + \gamma(900/(T+273))u_2(e_s - e_a)}{\Delta + \gamma(1 + 0.34u_2)} \quad (1)$$

where R_n is the net radiation at the crop surface (MJ m^{-2} d^{-1}), G is the soil heat flux density (MJ m^{-2} d^{-1}), γ is the psychrometric constant (kPa °C^{-1}), T is the daily air temperature (°C), u_2 is the daily wind speed at 2 m above ground (m s^{-1}), e_s is the saturation vapor pressure (kPa), e_a is the actual vapor pressure (kPa), Δ is the slope of the saturated vapor pressure in relation to air temperature (kPa °C^{-1}).

The solar radiation is calculated using the Angstrom formula (Maroufpoor *et al.* 2020), which has been proven to be suitable for daily global radiation estimation in China (Chen *et al.* 2004).

$$R_s = \left(a_s + b_s \frac{n}{N}\right) R_a \quad (2)$$

where R_s is the shortwave radiation (MJ m^{-2} d^{-1}), R_a is the extraterrestrial radiation (MJ m^{-2} d^{-1}), n is the actual duration of sunshine (h), N is the possible maximum duration of sunshine (h), a_s and b_s are two regression coefficients.

Differing from the previous studies which use the average value of coefficients a_s and b_s in the whole of China (Liu *et al.* 2010), we estimate the Angstrom coefficients using the measured radiation within the UYRB to ensure more accuracy and reliability. First, we use the formula given by the Penman–Montieth method to calculate the N and R_a based on date and latitude at 10 meteorological stations with radiation observation (see Figure 1 and Table 2). Secondly, we use nonlinear least-squares data fitting to estimate the a_s and b_s based on the observations of R_s and n. Thirdly, we use the Kriging interpolation method (Xu *et al.* 2006) to obtain a_s and b_s of those stations with no radiation observation.

Trend analysis method

The nonparametric Mann-Kendall (MK) test is highly recommended to analyze monotonic trends of hydrometeorological time series by the World Meteorological Organization (Zhang *et al.* 2018). In this study, it is used to identify temporal trends in ET_0 and other climatic variables. For a time series $X = \{x_1, x_2, \ldots, x_n\}$, the test statistic variable S is computed by:

$$S = \sum_{k=1}^{n-1} \sum_{j=k+1}^{n} sgn(x_j - x_k) \quad (3)$$

where n is the length (sample size) of the time series. We assume that the time-series data are independent and randomly distributed.

Table 1 | Information for the meteorological observatory stations used in this study

Subbasin	Station name	Latitude (°N)	Longitude (°E)	Altitude (m)	Station name	Latitude (°N)	Longitude (°E)	Altitude (m)
JSRB	Wudaoliang	35.22	93.08	4,612.2	Jiulong	29	101.5	7,987.3
	Tuotuohe	34.22	92.43	4,533.1	Zhaojue	28	102.85	2,132.4
	Zhiduo	33.85	95.6	4,179.0	Leibo	28.27	103.58	1,255.8
	Qumalai	34.13	95.78	4,175.0	Zhongdian	27.83	99.7	3,276.7
	Yushu	33.02	97.02	3,681.2	Yanyuan	27.43	101.52	2,545.0
	Qingshuihe	33.8	97.13	4,415.4	Xichang	27.9	102.27	1,590.9
	Shiqu	32.98	98.1	9,200.0	Zhaotong	27.35	103.72	1,949.5
	Dege	31.8	98.58	8,184.0	Lijiang	26.87	100.22	2,392.4
	Ganzi	31.62	100	8,393.5	Huaping	26.63	101.27	1,244.8
	Daofu	30.98	101.12	2,957.2	Panzhihua	26.58	101.72	1,190.1
	Batang	30	99.1	2,589.2	Huili	26.65	102.25	1,787.3
	Xinlong	30.93	100.32	8,000.0	Renhe	26.5	101.73	1,108.0
	Litang	30	100.27	3,948.9	Huize	26.42	103.28	2,110.5
	Qianning	30.48	101.48	3,449.0	Yuanmo	25.73	101.87	1,120.6
	Daocheng	29.05	100.3	8,727.7	Chuxiong	25.03	101.55	1,824.1
	Derong	28.72	99.28	7,422.9	Kunming	25	102.65	1,886.5
	Muli	27.93	101.27	2,426.5				
MTRB	Seda	32.28	100.33	8,893.9	Hanyuan	29.35	102.68	795.9
	Maerkang	31.9	102.23	2,664.4	Emeishan	29.52	103.33	8,047.4
	Xiaojin	31	102.35	2,369.2	Leshan	29.57	103.75	424.2
	Songpan	32.65	103.57	2,850.7	Yuexi	28.65	102.52	1,659.5
	Doujiangyan	31	103.67	698.5	Yibin	28.8	104.6	340.8
	Yaan	29.98	103	627.6	Banma	32.93	100.75	8,530.0
	Chengdu	30.67	104.02	506.1	Aba	32.9	101.7	3,275.1
	Ziyang	30.12	104.65	357.0	Neijiang	29.58	105.05	347.1
	Kangding	30.05	101.97	2,615.7				
JLRB	Wudu	33.4	104.92	1,079.1	Langzhong	31.58	105.97	382.6
	Pingwu	32.42	104.52	893.2	Bazhong	31.87	106.77	417.7
	Mianyang	31.45	104.73	522.7	Daxian	31.2	107.5	344.9
	Lveyang	33.32	106.15	794.2	Suining	30.5	105.55	355.0
	Guangyuan	32.43	105.85	513.8	Nanchong	30.78	106.1	309.7
	Wanyuan	32.07	108.03	674.0	Shapingba	29.58	106.47	259.1
WJRB	Pengshui	29.3	108.17	310.6	Meitan	27.77	107.47	792.2
	Youyang	28.83	108.77	664.1	Sinan	27.95	108.25	416.3
	Bijie	27.3	105.28	1,510.6	Qianxi	27.03	106.02	1,231.4
	Zunyi	27.7	106.88	843.9	Guiyang	26.58	106.73	1,223.8
MSB	Fengjie	31.02	109.53	299.8	Luzhou	28.88	105.43	334.8
	Badong	31.03	110.37	334.0	Tongzi	28.13	106.83	972.0
	Liangping	30.68	107.8	454.5	Xuyong	28.17	105.43	377.5
	Wanxian	30.77	108.4	186.7	Xishui	28.33	106.22	1,180.2
	Fuling	29.75	107.42	273.5	Jinfoshan	28.95	107.15	1,905.9

Table 2 | Estimation of the Angstrom coefficient for 10 stations with radiation observation

Station	a_s	b_s	Station	a_s	b_s
Emeishan	0.23	0.51	Mianyang	0.17	0.47
Guiyang	0.19	0.50	Nanchong	0.18	0.48
Kunming	0.21	0.48	Panzhihua	0.14	0.58
Leshan	0.18	0.48	Zhaotong	0.16	0.64
Lijiang	0.25	0.49	Chongqing	0.14	0.56

When the length of the time series is greater than 10, the normalized variable of S is given by:

$$Z = \begin{cases} \dfrac{S-1}{\sqrt{Var(S)}} & S > 0 \\ 0 & S = 0 \\ \dfrac{S+1}{\sqrt{Var(S)}} & S < 0 \end{cases} \quad (4)$$

when $Z < 0$, the time series is identified as an upward trend. When $Z > 0$, the time series is identified as a downward trend. When $|Z| \geq Z_{\alpha/2}$, the monotonic trend is believed to be significant at the significance level of α.

Attribution analysis method

To explore the causes of ET_0 change, an attribution analysis method (Figure 2) is proposed in this study as follows: (1) The abrupt change points in climatic variable series are detected by using the time-series analysis method. (2) The climatic variable series are reconstructed based on the abrupt change analysis results to obtain stationary series. (3) ET_0 is recalculated by using the reconstructed series for one climatic variable, while original data for other variables are retained. The difference between the recalculated ET_0 and original ET_0 is considered as the contribution of this climatic variable to ET_0 change.

Abrupt change analysis

The nonparametric Pettitt test (Pettitt 1979) is employed in this study. The abrupt change point of the climatic variable series is detected by the Pettitt test, which judges whether there is a significant difference in the cumulative distribution function before and after the point. For the climatic variable series $X = \{x_1, x_2, \ldots, x_n\}$, the Mann–Whitney statistic variable is calculated to test whether the samples $x_1, x_2, \ldots, x_t$ and $x_{t+1}, x_{t+2}, \ldots, x_n$ belong to the same population. The Mann–Whitney statistic variable $U_{t,n}$ (Zhang *et al.* 2018) is given by:

$$U_{t,n} = U_{t-1,n} + \sum_{j=1}^{n} \operatorname{sgn}(x_i - x_j) \tag{5}$$

where $t = 2, \ldots, n$. The point, which has the maximum $U_{t,n}$ value, can be considered as the change. The significance of the change point can be tested by:

$$P = 2\exp\{-6(k_n)^2/(n^3 + n^2)\} \tag{6}$$

where P denotes the significance of change point, and k_n denotes the maximum $U_{t,n}$ value.

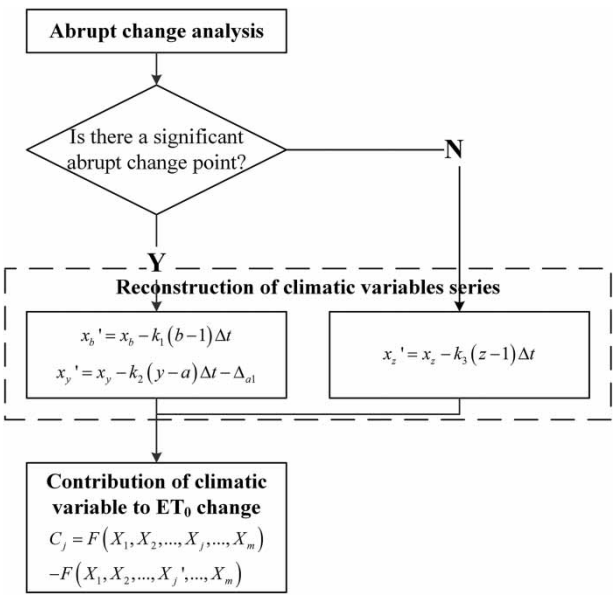

Figure 2 | Flow chart of the attribution analysis method.

Reconstruction of climatic variables series

When there is a significant abrupt change point in a climatic variable series, the subseries before the abrupt change point is defined as the baseline series. The subseries after this abrupt change point is defined as the altered series. We replace the original data with the detrended data to obtain the reconstructed series. For the climatic variable series $X = \{x_1, x_2, \ldots, x_n\}$, after the trend and slope being analyzed by using the MK test, the reconstructed climatic variable series is given by:

$$x_b' = x_b - k_1(b-1)\Delta t \tag{7}$$

$$x_y' = x_y - k_2(y-a)\Delta t - \Delta_{a1} \tag{8}$$

where a $(1 < a < n)$ is the significant abrupt change point (year); $b = 1, \ldots, a$; x_b is the original value at time b (year); x_b' is the detrended value (mm); k_1 is the slope during baseline period (mm/year); $y = a + 1, \ldots, n$ (year); x_y (mm) is the original value at time y; x_y' is the detrended value (mm); k_2 is slope during altered period (mm/year); Δt is the time step (year); Δ_{a1} is the difference between original value at time a and time 1 (year).

When there is not a significant abrupt change point in the climatic variable series, it suggests that no abrupt change has occurred or the abrupt point occurred before the study period. We replace the original data during the entire study period with the detrended data to obtain the reconstructed series. After the trend and slope being analyzed, the reconstructed climatic variable series is given by:

$$x'_z = x_z - k_3(z-1)\Delta t \tag{9}$$

where $z = 1, \ldots, n$, x_z is the original value at time z (year); x'_z is the detrended value (mm); k_3 is the slope during the entire study period (mm/year).

Contribution of climatic variable to ET_0 change

ET_0 is regarded as a function of related climatic variables (e.g., T, RH, WS, and SD), which is described by the Penman–Montieth method. The ET_0 is written as:

$$ET_0 = F(X_1, X_2, \ldots, X_j, \ldots, X_m) \tag{10}$$

where $F(\cdot)$ is the function of the Penman–Montieth method; $X_1, X_2, \ldots, X_j, \ldots, X_m$ are the related climatic variables. Then, the contribution of climatic variable X_j to ET_0 change is calculated by:

$$C_j = F(X_1, X_2, \ldots, X_j, \ldots, X_m) - F(X_1, X_2, \ldots, X'_j, \ldots, X_m) \tag{11}$$

where C_j is the contribution series of climatic variable X_j to ET_0 change; X'_j is the reconstructed series of climatic variable X_j. We use the slope value of the contribution series to represent the contribution of climatic variable to ET_0 change.

Sensitivity analysis method

Besides the change amount of climate variables, the sensitivity of ET_0 to climate variables has an important influence on ET_0 change. A small change in sensitive climatic factor may result in a great change in ET_0. To better understand the attribution results, the sensitivity analysis of ET_0 to climate variables is performed. A simple and widely used method is to compute and plot the relative changes of an input variable against the resultant relative change of the output variable as a curve, from which the sensitivities are easily read and compared (Liu *et al.* 2020; Zhang *et al.* 2020; Wang *et al.* 2021).

RESULTS

Spatial distributions of annual ET_0 and related climatic variables

Daily ET_0 is calculated by using the Penman–Montieth method at the 80 stations. Annual ET_0 is further calculated by accumulating the daily values. We plot the spatial distribution of mean annual ET_0 as shown in Figure 3. The annual ET_0 of the UYRB has an inhomogeneous spatial pattern with low values in the eastern part of the basin, high values in the western part, and very high values in the southwestern part. The spatial distributions of the annual values of four related meteorological variables (i.e., SD, T, RH, and WS) are plotted in Figure 4. We find SD values in the western part of the UYRB, which are obviously larger than those in the eastern part. There is a distinct boundary between the western and eastern parts. From low to high value, a clear northwestern-southeastern gradient is found in the spatial distributions of T and RH. Differing from the other climatic variables, the spatial distribution of WS is

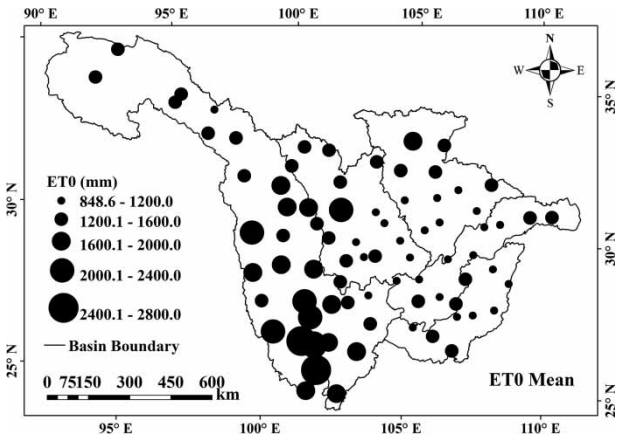

Figure 3 | Mean annual ET_0 of the UYRB during 1951–2020.

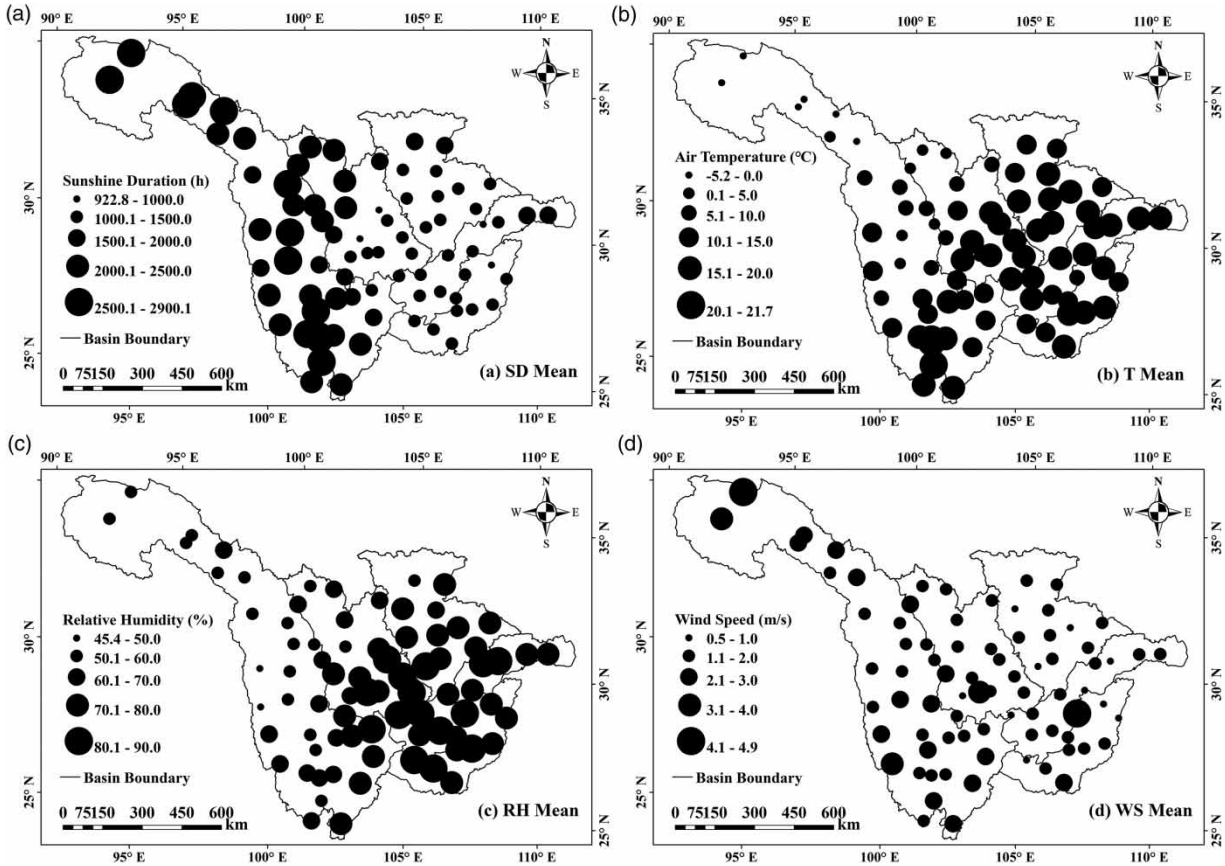

Figure 4 | Mean annual climatic variables of the UYRB during 1951–2020: (a) sunshine duration, (b) air temperature, (c) relative humidity, and (d) wind speed.

relatively homogeneous except for a few isolated stations having high values. The integrated views of Figures 3 and 4 show the combined effects of SD, *T*, RH, and WS on ET_0. It can be seen that the highest ET_0 values occur in the southwestern part, where the SD value and *T* value are very high. Meanwhile, the lowest ET0 values found in the central region (southeast of the MTRB, south of JLRB, middle of the MSB) are the lowest, where the lowest SD, high *T* values and low WS values are observed. In general, the spatial pattern of ET_0 in the UYRB is mainly due to the very high SD, very low RH, and high WS in the west, and the very low SD, very high RH, and low WS in the east.

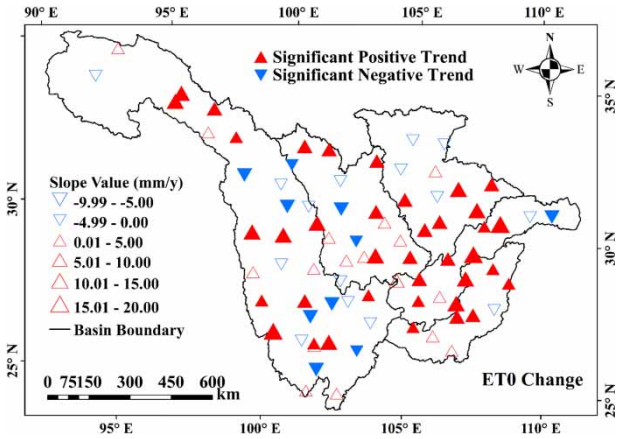

Figure 5 | Annual trend slopes and the MK test result (at the 95% confidence level) of ET_0 during 1951–2020.

ET_0 trend

The trends for the annual ET_0 during 1951–2020 are tested by using the MK test and plotted in Figure 5. The red upward triangles represent positive trends, and the blue downward triangles represent negative trends. Sizes of triangles indicate the magnitudes of change slopes. Solid triangles indicate significant trends with confidence level

higher than 95% (Zhang *et al.* 2018). It can be seen that the change of ET_0 has complex spatial variability in the UYRB. There are 55 stations presenting increasing trends in annual ET_0 (i.e., 69% of all stations), of which 38 stations (i.e., 48% of all stations) are statistically significant at 95% confidence level. Decreasing trends are detected in 25 stations (i.e., 31% of all stations), of which 10 stations (i.e., 12.5% of all stations) are dominated by significant negative trends at 95% confidence level. Annual ET_0 of the UYRB shows an upward trend in general. The significant increases of annual ET_0 gather in the central region of the UYRB, where the mean annual ET_0 is low. The stations showing negative trends mainly distribute in the upper Yalong River, lower Jinsha River, upper Jiangling River, and Middle Minjiang River.

Trends of the area-averaged ET_0 in the UYRB and the subbasins are also analyzed by using the MK test. The results are summarized in Table 3. The area-averaged ET_0 of the UYRB has a significant increasing trend at confidence level of 95%, with a slope of 3.3 mm/year. ET_0 in the JSRB, MTRB, JLRB, WJRB, and MSB all show increasing trends, with slopes of 2.9, 2.9, 3.9, 3.0, and 4.9 mm/year, respectively. The results are consistent in the subbasins except that the confidence level is lower than 95%.

Climate factors for ET_0 change

Trends of SD, *T*, RH, and WS are also analyzed to understand the causal mechanism behind the changes of ET_0. The results of trend analysis for annual climatic variables and their spatial patterns are shown in Figures 6. Beginning with the annual *T*, it can be seen that obvious warming trends have occurred across the entire UYRB. This is consistent with global warming reported in most parts of the world. There are 70 stations presenting positive trends in annual *T* (i.e., 87.5% of all stations), among which 61 stations (i.e., 76% of all stations) are statistically significant at 95% confidence level. The largest increasing trends (greater than 0.04 °C/year) mainly distribute in the western part of the UYRB, while smaller positive trends (around or less than 0.03 °C/year) occur in the eastern part. Contrarily, although increasing trends are observed in a few stations distributed in the western part, the annual SD of the UYRB shows an upward trend in general. Sixty-five stations (i.e., 81% of all stations) present decreasing trends, with most trends being greater than 4 h/year. Among these stations, decreases in 47 stations (i.e., 59% of all stations) are statistically significant. Similar changes are detected in the annual RH. Fifty-nine stations (i.e., 74% of all stations) show decreasing trends, and half of them are statistically significant. The annual RH has the least number of statistically significant trends. There are 26 stations having significant negative trends and 7 stations having significant positive trends. The annual WS shows mixed increasing and decreasing trends in the entire UYRB, which does not have an obvious trend pattern. There are 54 stations (i.e., 67.5% of all stations) showing decreasing trends, and most of them are statistically significant.

Table 3 | Trends of area-averaged ET_0 in the UYRB and subbasins

Basin/subbasin	Trend	Slope (mm/year)	Confidence level (%)
UYRB	↑	3.3	95
JSRB	↑	2.9	95
MTRB	↑	2.9	99
JLRB	↑	3.9	99
WJRB	↑	3.0	–
MSB	↑	4.9	95

Note: '–' represents a confidence level lower than 95%.

Contributions to ET_0 trend

The proposed attribution analysis method is employed for the UYRB and all subbasins to evaluate the effects of changes of climatic variables on ET_0. Abrupt change analysis is first done for area-averaged climatic variable series in the UYRB and each subbasin. The abrupt change points and corresponding confidence levels are listed in Table 4. In this study, the abrupt change points at the confidence level of 95% or more are considered as significant. The *T* series, RH series, and WS series can be divided into subseries by the abrupt change points. We then do the Pettitt test on the subseries. The results show that there are no significant abrupt change points in the subseries, indicating the absence of multiple change points in the climatic variable series. Then, following the steps of the proposed method, the climatic variable series are reconstructed according to the abrupt change analysis results,

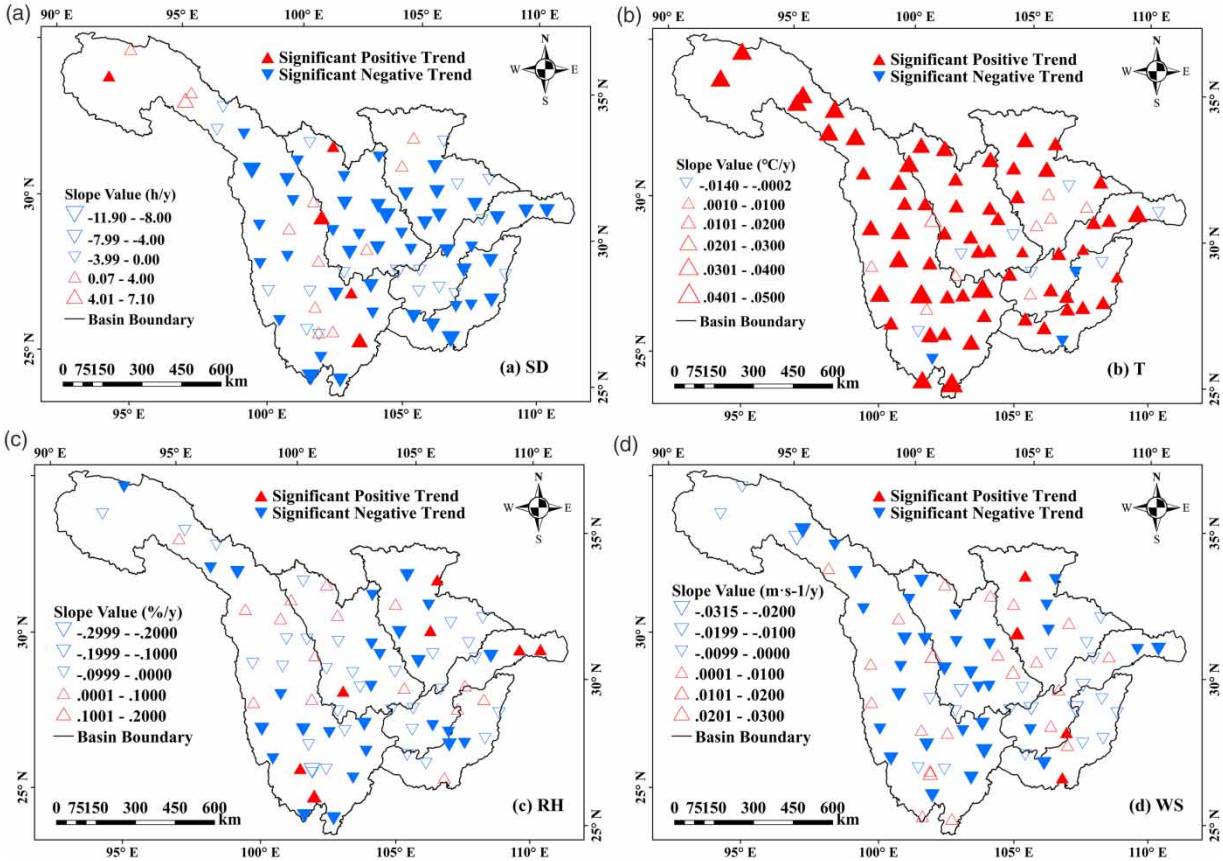

Figure 6 | Annual trend slopes and the MK test result (at the 95% confidence level) of climatic variables during 1951–2020: (a) sunshine duration, (b) air temperature, (c) relative humidity, and (d) wind speed.

Table 4 | Abrupt change points of climatic variable series in the UYRB and subbasins

	Abrupt change point (confidence level)			
Subbasin	**SD**	**T**	**RH**	**WS**
UYRB	1988 (–)	1997 (99%)	2000 (99%)	1991 (99%)
JSRB	1988 (–)	1997 (99%)	2002 (99%)	1993 (99%)
MTRB	1988 (–)	1997 (99%)	2000 (99%)	1991 (99%)
JLRB	1996 (–)	1996 (99%)	1996 (99%)	2002 (99%)
WJRB	1993 (–)	1997 (–)	2003 (–)	1999 (99%)
MSB	1997 (–)	1997 (99%)	2000 (99%)	1997 (–)

Note: '–' represents a confidence level lower than 95%.

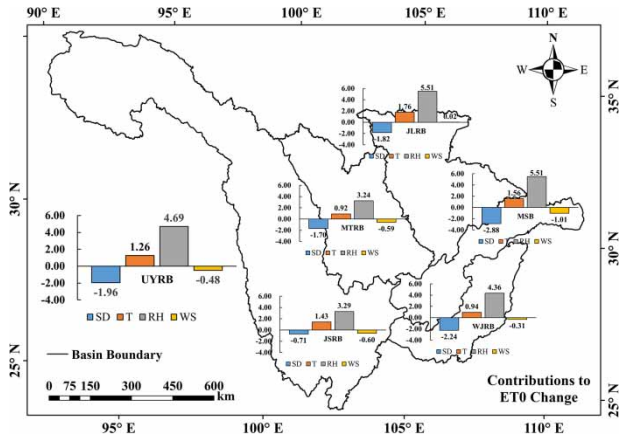

Figure 7 | Contributions of climatic variables to ET_0 change in the UYRB and subbasins.

and contributions to ET_0 change are calculated. The contributions of climatic variables to ET_0 change are shown in Figure 7. It can be found that ET_0 change results from the combined effect of the climatic variables and the contributions vary in different subbasins. For the five subbasins and entire UYRB, RH has the dominant influence on ET_0 change. RH decrease tends to increase ET_0, causing 3.29, 3.24, 5.51, 4.36, and 5.51 mm/year of ET_0 increase in the JSRB, MTRB, JLRB, WJRB, and MSB, respectively. The

decreasing SD contributes to decrease ET_0 in the subbasins and entire UYRB. SD takes the second place of contributions of climatic variables to ET_0 change in MTRB, JLRB, WJRB, MSB, and the entire UYRB. Impacts of SD on ET_0 in the eastern part of UYRB are more evident in the western part. The increasing T is mainly responsible for the increasing trends in ET_0 in the UYRB. Impacts of T on ET_0 are more evident in the JSRB, where T is the second dominant factor. WS has the least contribution among selected climatic variables in the UYRB. The influence of WS is more complex than others in space. Changes in WS contribute to decrease ET_0 in the subbasins and entire UYRB except the JLRB, where WS tends to increase ET_0.

Sensitivity of the ET_0 to climatic variables

T has a significant trend in the UYRB but takes the third place in terms of contribution to ET_0 change. Therefore, sensitivity analysis is conducted by using the sensitivity curve method to further explore the causes of ET_0 change. Scenarios with $X_j + 0\%$ of X_j, $X_j \pm 10\%$of X_j, $X_j \pm 20\%$ of X_j, and $X_j \pm 30\%$ of X_j are generated for the climate variables and used as the input for the Penman–Montieth method. The corresponding relative changes of ET_0 against the relative changes of climate variables in the UYRB and subbasins are plotted in Figure 8. At the same relative change value of climate variable, the larger corresponding relative change of ET_0 means the stronger sensitivity of the ET_0 to climate variable. It can be seen that the sensitivities vary in climate variables and space, but the general law is consistent. Positive correlations are identified between relative change of ET_0 and relative change of SD, T and WS in the UYRB and subbasins, while negative correlations are identified between relative change of ET_0 and relative change of RH. This means RH decrease and T increase tend to increase ET_0, while SD decrease and WS decrease tend to decrease ET_0. The results of sensitivity analysis are in accordance with the results of attribution analysis. In the entire UYRB and subbasins, relative change from −30 to 30% in SD, T, RH, and WS can result in relative change from −8 to 7, −3 to 2, 14 to −15, and −7 to 4% in ET_0. RH is the most sensitive factor although the sensitivity degree varies in different subbasins. This is consistent with results of previous studies conducted in the Yangtze River Basin (Gong *et al.* 2006; Xu *et al.* 2006) and in all climate regions of China (Yin *et al.* 2010). The impacts of climatic variables on ET_0 depend not only on their change slopes but also the sensitivities. The sensitivity of ET_0 to T is the lowest in the entire UYRB and subbasins. Therefore, it is easy to explain why T variables present larger change slopes but provide small contribution in ET_0 increase.

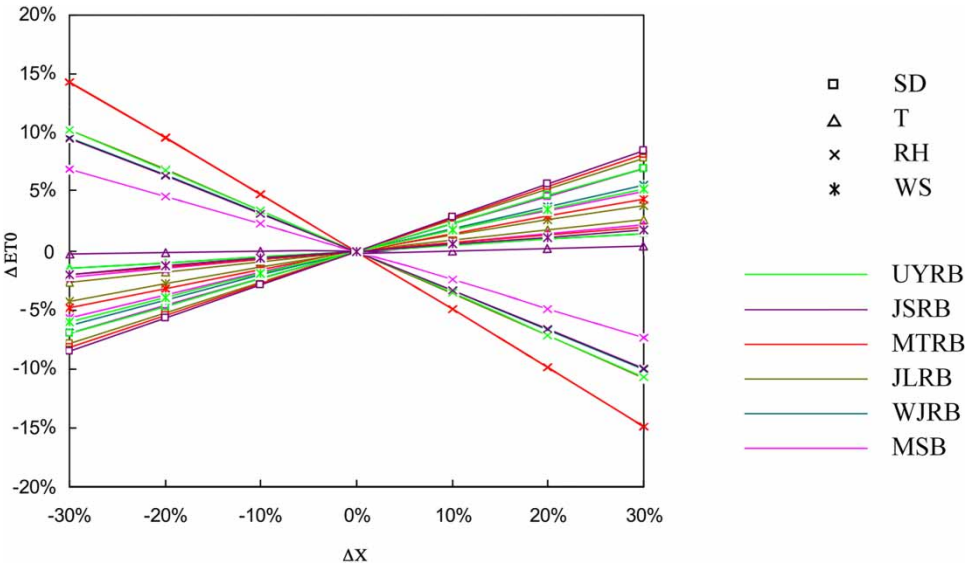

Figure 8 | Sensitivity of ET_0 to climatic variables in the UYRB and subbasins.

DISCUSSION

In this study, the series reconstruction method for climatic variable is different from the previous studies (Xu *et al.* 2006; Wang *et al.* 2012). As mentioned in the 'Introduction' section, the traditional recovered stationary series method used in previous studies reconstruct the climatic variable series by the trend and slope of the whole series, without considering whether there is an abrupt change point. In fact, when there is an abrupt change point in one climatic variable series, the subseries before and after abrupt change point commonly have different trends and slopes. In this case, the traditional recovered stationary series method will misestimate the changes in variable series. What's worse, in most cases, subseries before abrupt change point is flatter, and the traditional method will mean this subseries has an opposite trend to the actual situation. We use the example of the T in MTRB for illustration (Figure 9). An abrupt change has been detected in the year 1997 (Table 4). It can be seen from Figure 9(a) that the original T series has an upward trend with a slope of 0.0151 °C /year. Two subseries also show upward trends. Slopes of the two series are 0.0009 and 0.0157 °C /year. The subseries (1951–1997) is flatter than the subseries (1998–2020). We reconstruct the original T series using the traditional recovered stationary series method, as shown in Figure 9(b). It can be seen that the reconstructed subseries (1951–1997) shows a decreasing trend, which is contrary to the actual situation. Results of the improved method are shown in Figure 9(c). It can be seen that the original T series is better detrended. Both subseries recover stationary. The study period in this work is much longer than the studies mentioned above, using the proposed series reconstruction method obtains more reliable results. It is worth noting that this proposed method is also applicable when there are multiple change points. When there are N significant abrupt change points in the original series, we divide the original series into N +1 subseries and reconstruct each subseries using the proposed method. In addition, other forcings than the studied ones (i.e., RH, T, SD, and

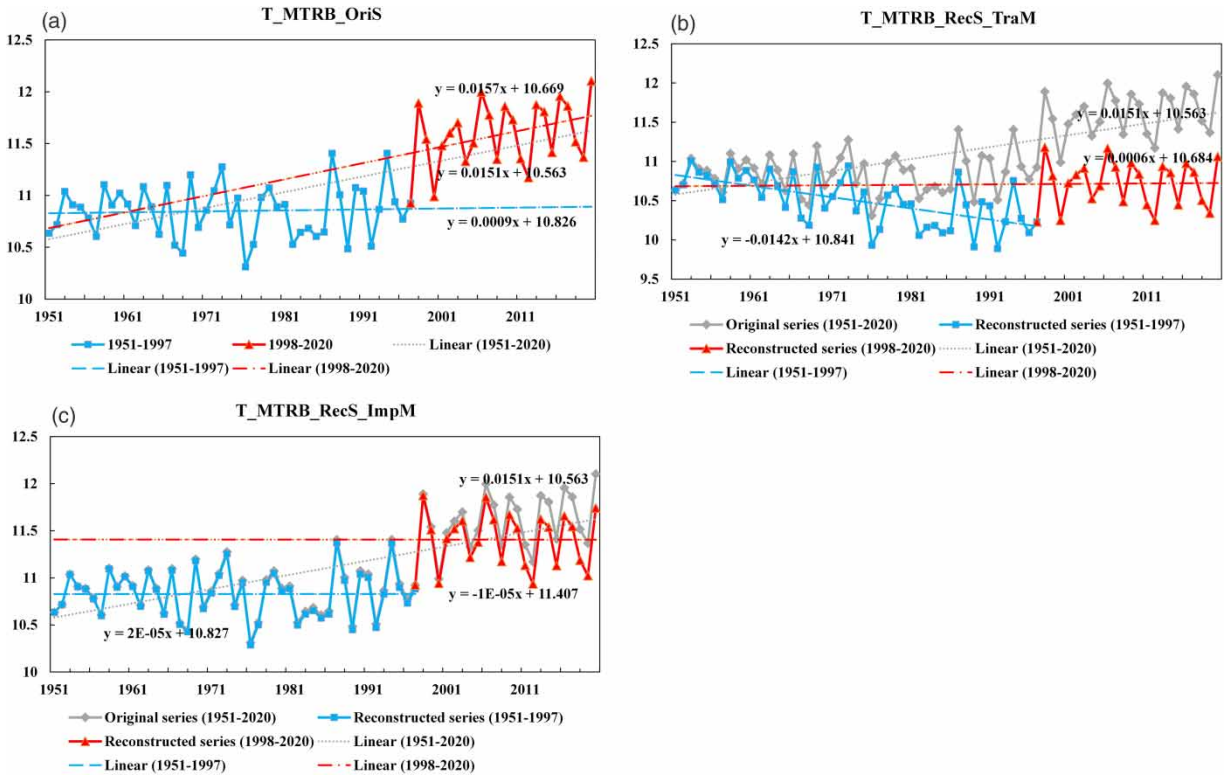

Figure 9 | Original series and reconstructed series of T in MTRB: (a) original series; (b) reconstructed series by the traditional recovered stationary series method; (c) reconstructed series by an improved method.

WS) are not considered in the proposed method. This restriction is justified but is possible to overestimate the contributions of RH, *T*, SD, and WS.

CONCLUSIONS

In this study, we estimate the ET_0 in 80 meteorological observatory stations within the UYRB during 1951–2020 by using the Penman–Monteith method. The spatial distributions of ET_0 and ET_0 trend are studied to describe the spatial characteristics of ET_0 change. Trends of the area-averaged ET_0 in the subbasins and entire UYRB are also analyzed to describe the temporal characteristics. An attribution analysis method is proposed to quantify the impacts of changes in climatic variables on ET_0. The sensitivity analysis is conducted to further explore the causes of ET_0 change.

The UYRB has an irreplaceable position and inestimable value in China's strategic reserve of water resources and hydropower resources, which is vulnerable and sensitive to changing environment. This study aims to provide a newer and more detailed description of ET_0 change at basin and subbasin scales in the UYRB, which provides evidence of current climate change occurring and historic trends. Special efforts are also made in the attribution of ET_0 change, which offers guidance on adaptive regulation of water resources systems under climate change.

Several important findings are revealed in the UYRB. During 1951–2020, ET_0 increases significantly by 3.3 mm/year in the entire UYRB. Stations with significant increases in annual ET_0 are concentrated in the central part of the UYRB, where the mean annual ET_0 is low. The stations showing negative trends are mainly distributed in the upper Yalong River, lower Jinsha River, upper Jiangling River, and middle Minjiang River. Relative humidity has the dominant influence on ET_0 change. Relative humidity decrease tends to increase ET_0, causing 4.69 mm/year of ET_0 increase in the entire UYRB. Temperature increase tends to increase ET_0, while sunshine duration decrease and wind speed decrease contribute to decrease ET_0 in the UYRB. Contributions of climatic variables to ET_0 change vary in subbasins.

Seasonal patterns of ET_0 changes and their causes have not been analyzed in this work. Seasonal trends in ET_0 are possible to have a great impact on water resources planning and management due to seasonal behaviors of water resources allocation such as irrigation. Therefore, we are doing another detailed study on seasonal ET_0 changes and their impacts as a follow-up study to this paper.

ACKNOWLEDGMENTS

This work is supported by the China Postdoctoral Science Foundation (Grant No. 2019M661884); the Natural Science Foundation of Jiangsu Province, China (Grant No. BK20200160); and the Special Research Fund of Nanjing Hydraulic Research Institute (Grant No. Y120006).

DATA AVAILABILITY STATEMENT

All relevant data are included in the paper or its Supplementary Information.

REFERENCES

Akhavan, S., Kanani, E. & Dehghanisanij, H. 2019 Assessment of different reference evapotranspiration models to estimate the actual evapotranspiration of corn (*Zea mays* L.) in a semiarid region (case study, Karaj, Iran). *Theoretical and Applied Climatology* **137** (1–2), 1403–1419.

Chen, R. S., Kang, E. S., Yang, J. P., Lu, S. H. & Zhao, W. Z. 2004 Validation of five global radiation modes with measured daily data in China. *Energy Conversion Management* **45**, 1759–1769.

Dakhlaoui, H., Seibert, J. & Hakala, K. 2020 Sensitivity of discharge projections to potential evapotranspiration estimation in Northern Tunisia. *Regional Environmental Change* **20** (2), 34.

Ghorbani, M. A., Kazempour, R., Chau, K. W., Shamshirband, S. & Ghazvinei, P. T. 2018 Forecasting pan evaporation with an integrated artificial neural network quantum-behaved particle swarm optimization model: a case study in Talesh, Northern Iran. *Engineering Applications of Computational Fluid Mechanics* **12** (1), 724–737.

Gong, L. B., Xu, C. Y., Chen, D. L., Halldin, S. & Chen, Y. Q. D. 2006 Sensitivity of the Penman-Monteith reference evapotranspiration to key climatic variables in the Changjiang (Yangtze River) basin. *Journal of Hydrology* **329**, 620–629.

Guo, D. L., Westra, S. & Maier, H. R. 2016 An R package for modelling actual, potential and reference evapotranspiration. *Environmental Modelling & Software* **78**, 216–224.

Jing, W., Yaseen, Z. M., Shahid, S., Saggi, M. K., Tao, H., Kisi, O., Salih, S. Q., Al-Ansari, N. & Chau, K. W. 2019 Implementation of evolutionary computing models for reference evapotranspiration modeling: short review, assessment and possible future research directions. *Engineering Applications of Computational Fluid Mechanics* **13** (1), 811–823.

Liu, Q., Yang, Z. F., Cui, B. S. & Sun, T. 2010 The temporal trends of reference evapotranspiration and its sensitivity to key meteorological variables in the Yellow River Basin, China. *Hydrological Processes* **24** (15), 2171–2181.

Liu, D., Mishra, A. K. & Ray, D. K. 2020 Sensitivity of global major crop yields to climate variables: a non-parametric elasticity analysis. *Science of the Total Environment* **748**, 141431.

Malik, A., Kumar, A., Kim, S., Kashani, M. H., Karimi, V., Sharafati, A., Ghorbani, M. A., Al-Ansari, N., Salih, S. Q., Yaseen, Z. M. & Chau, K. W. 2020 Modeling monthly pan evaporation process over the Indian central Himalayas: application of multiple learning artificial intelligence model. *Engineering Applications of Computational Fluid Mechanics* **14** (1), 323–338.

Maroufpoor, S., Bozorg-Haddad, O. & Maroufpoor, E. 2020 Reference evapotranspiration estimating based on optimal input combination and hybrid artificial intelligent model: hybridization of artificial neural network with grey wolf optimizer algorithm. *Journal of Hydrology* **588**, 125060.

Nagler, P. L., Glenn, E. P., Nguyen, U., Scott, R. L. & Doody, T. 2013 Estimating Riparian and Agricultural Actual Evapotranspiration by Reference Evapotranspiration and MODIS Enhanced Vegetation Index. *Remote Sensing* **5** (8), 3849–3871.

Nourani, V., Elkiran, G. & Abdullahi, J. 2019 Multi-station artificial intelligence based ensemble modeling of reference evapotranspiration using pan evaporation measurements. *Journal of Hydrology* **577**, 123958.

Penman, H. L. 1956 Evaporation: an introductory survey. *Netherlands Journal of Agricultural Science* **4**, 9–29.

Pettitt, A. N. 1979 A non-parametric approach to the change-point detection. *Journal of Applied Statistics* **28**, 126–135.

Pour, S. H., Abd Wahab, A. K., Shahid, S. & Bin Ismail, Z. 2020 Changes in reference evapotranspiration and its driving factors in peninsular Malaysia. *Atmospheric Research* **246**, 105096.

Qasem, S. N., Samadianfard, S., Kheshtgar, S., Jarhan, S., Kisi, O., Shamshirband, S. & Chau, K. W. 2019 Modeling monthly pan evaporation using wavelet support vector regression and wavelet artificial neural networks in arid and humid climates. *Engineering Applications of Computational Fluid Mechanics* **13** (1), 177–187.

Qi, J., Wang, L., Zhou, J., Song, L., Li, X. P. & Zeng, T. 2019 Coupled snow and frozen ground physics improves cold region hydrological simulations: an evaluation at the upper Yangtze River Basin (Tibetan Plateau). *Journal of Geophysical Research-Atmospheres* **124** (23), 12985–13004.

Qin, P. C., Xu, H. M., Liu, M., Xiao, C., Forrest, K. E., Samuelsen, S. & Tarroja, B. 2020 Assessing concurrent effects of climate change on hydropower supply, electricity demand, and greenhouse gas emissions in the Upper Yangtze River Basin of China. *Applied Energy* **279**, 115694.

Sippel, S., Meinshausen, N., Fischer, E. M., Szekely, E. & Knutti, R. 2020 Climate change now detectable from any single day of weather at global scale. *Nature Climate Change* **10** (1), 35–41.

Song, X. Y., Lu, F., Xiao, W. H., Zhu, K., Zhou, Y. Y. & Xie, Z. B. 2018 Performance of 12 reference evapotranspiration estimation methods compared with the Penman-Monteith method and the potential influences in northeast China. *Meteorological Applications* **26** (1), 83–96.

Thornthwaite, C. W. 1948 An approach toward a rational classification of climate. *Geographical Review* **38**, 55–94.

Wang, Y., Jiang, T., Bothe, O. & Fraedrich, K. 2007 Changes of pan evaporation and reference evapotranspiration in the Yangtze River basin. *Theoretical and Applied Climatology* **90** (1–2), 13–23.

Wang, W. G., Shao, Q. X., Peng, S. Z., Xing, W. Q., Yang, T., Luo, Y. F., Yong, B. & Xu, J. Z. 2012 Reference evapotranspiration change and the causes across the Yellow River Basin during 1957–2008 and their spatial and seasonal differences. *Water Resources Research* **48** (5), 113–122.

Wang, H. N., Lv, X. Z. & Zhang, M. Y. 2021 Sensitivity and attribution analysis of vegetation changes on evapotranspiration with the Budyko framework in the Baiyangdian catchment, China. *Ecological Indicators* **120**, 106963.

Weiland, F. C. S., Tisseuil, C., Durr, H. H., Vrac, M. & van Beek, L. P. H. 2012 Selecting the optimal method to calculate daily global reference potential evaporation from CFSR reanalysis data for application in a hydrological model study. *Hydrology and Earth System Sciences* **16** (3), 983–1000.

Xu, C.-Y. & Singh, V. P. 2002 Cross-comparison of mass-transfer, radiation and temperature based evaporation models. *Water Resources and Management* **16**, 197–219.

Xu, C. Y., Gong, L., Jiang, T., Chen, D. & Singh, V. P. 2006 Analysis of spatial distribution and temporal trend of reference evapotranspiration and pan evaporation in Changjiang (Yangtze River) catchment. *Journal of Hydrology* **327** (1–2), 81–93.

Yaseen, Z. M., Al-Juboori, A. M., Beyaztas, U., Al-Ansari, N., Chau, K. W., Qi, C. C., Ali, M., Salih, S. Q. & Shahid, S. 2020 Prediction of evaporation in arid and semi-arid regions: a comparative study using different machine learning models. *Engineering Applications of Computational Fluid Mechanics* **14** (1), 70–89.

Yin, Y., Wu, S., Chen, G. & Dai, E. 2010 Attribution analyses of potential evapotranspiration changes in China since the 1960s. *Theoretical and Applied Climatology* **101**, 19–28.

Zhang, Y., Zhong, P. A., Wang, M. L., Xu, B. & Chen, J. 2018 Changes identification of the Three Gorges reservoir inflow and the driving factors quantification. *Quaternary International* **475**, 28–41.

Zhang, Y., Wang, M. L., Chen, J., Zhong, P. A., Wu, X. F. & Wu, S. Q. 2020 Multiscale attribution analysis for assessing effects of changing environment on runoff: case study of the Upstream Yangtze River in China. *Journal of Water and Climate Change*. https://doi.org/10.2166/wcc.2020.155.

Zhong, W. J., Guo, J., Chen, L., Zhou, J. Z., Zhang, J. H. & Wang, D. W. 2020 Future hydropower generation prediction of large-scale reservoirs in the upper Yangtze River basin under climate change. *Journal of Hydrology* **588**, 125013.

First received 11 January 2021; accepted in revised form 1 April 2021. Available online 13 April 2021